Energy-Spectral Efficiency Optimization in Vehicular Communications: Joint Clustering and Pricing-Based Robust Power Control Approach

Yuan-ai Xie, Zhixin Liu, *Member, IEEE*, Kit Yan Chan, *Member, IEEE*, and Xinping Guan, *Fellow, IEEE*

***Abstract*—Smart, and green cities impose stringent requirements on spectral efficiency (SE), and energy efficiency (EE) of vehicular networks. For the current vehicular ad-hoc networks (VANETs), vehicle's mobility leads to rapid topology changes, and high channel uncertainty. However, clustering schemes for establishing stable clusters, and robust power control (RPC) combating with channel fluctuation are investigated independently. In this paper, joint clustering, and RPC schemes are proposed to optimize the SE, and EE of the involved VANETs. Via the same fixed-length slot, the synchronized interference constraints of cluster heads (CHs) are formed, and offer conditions for RPC. Due to the random channel fluctuations, all CHs' synchronized interference constraints are formulated as probability constraints. Besides, a pricing-based utility which avoids the separate optimization between SE, and EE is introduced, and the price's impact on the tradeoff between them is involved. Since the probability constraints are intractable, and the unified utility is nonconvex, the Bernstein approximation, and successive convex approximation (SCA) are used to transform the problem into a tractable convex one. Through dual decomposition, two RPC algorithms are proposed to determine the optimal solutions for the fixed price C, and the optimal price C^*, respectively. Numerical simulations are used to evaluate the algorithmic performances in high-dynamic system, and the results show that the proposed algorithms are effective. The validity of the clustering method, and the proposed RPC scheme is further verified by comparisons.**

***Index Terms*—Energy efficiency, spectral efficiency, VANETs, clustering, time scheduling, channel uncertainty, robust power control.**

I. Introduction

LATELY vehicular communications have aroused a great concern due to its potential to improve autonomous driving performance, user experience and traffic efficiency [1]–[3]. In vehicular ad-hoc networks (VANETs), the frequent and extensive topological changes caused by vehicles' mobility require a large amount of state information exchange. Besides, higher data rates for vehicles are desired to avoid information loss and ensure traffic safety. Hence, it is necessary to maximize the sum rates of the whole vehicular network. In view of the limited spectrum resources, spectral efficiency (SE) maximization is pursued instinctively in the design of the vehicular communication systems. To create smart green cities, green vehicular network focusing on energy efficiency (EE) maximization and improving travel efficiency is also necessary [4], [5]. Thus, EE is another performance indicator that needs to be considered in the systems design.

There are two mainstream solutions for vehicular communications, i.e., ad-hoc communication over the 802.11p standard and backend-based communication Long Term Evolution (LTE) cellular network [6], [7]. Although the fresh LTE cellular network has these advantages (e.g., broad coverage and strong robustness) that ad-hoc doesn't have, it also has some obvious deficiencies (e.g., high latency and weak network security defense), which can be perfectly compensated by the mature VANETs [8], [9]. Therefore, cooperative communication is a better solution in vehicular network. Particularly due to vehicle to vehicle (V2V) links have more complex mobile environments than vehicle to infrastructure (V2I) links, this paper detailedly studies V2V links based on VANETs.

As the key feature of VANETs, high mobility leads to frequent topology changes, unstable communications. In fact, Clustering facilitates stable and scalable network structures and communications [10]; Robust power control (RPC) schemes can achieve more stable performance output (SE, EE and real time outage of links) under the mobile channel fluctuation [11]. Based on these evidences, the joint clustering and RPC schemes are crucial.

A. Related Works

In VANETs, Time Division Multiple Access (TDMA) is widely used and assigns the collision-free spectrum resources to different vehicles by a flexible time-slot scheduling [12]. There are some flexible TDMA-based protocols which avoid the wastage and shortage of the fixed-length time slot [13], [14]. In [13], the frame length is dynamically doubled or halved based on the vehicle density, but the overhead is very high.

Manuscript received March 27, 2020; revised June 20, 2020; accepted August 30, 2020. Date of publication September 3, 2020; date of current version November 12, 2020. This work was supported in part by the National Natural Science Foundation of China under Grants 61873223 and 61973264, and in part the Natural Science Foundation of Hebei Province under Grant F2019203095. The review of this article was coordinated by Dr. X. Dong. *(Corresponding author: Zhixin Liu.)*

Yuan-ai Xie and Zhixin Liu are with the School of Electrical Engineering, Yanshan University, Qinhuangdao 066004, China (e-mail: xieyuan_ai@163.com; lzxauto@ysu.edu.cn).

Kit Yan Chan is with the School of Electrical Engineering, Computing, and Mathematical Sciences, Curtin University Perth, WA 6102, Australia (e-mail: kit.chan@curtin.edu.au).

Xinping Guan is with the School of Electronic Information and Electrical Engineering, Shanghai Jiaotong University, Shanghai 200240, China (e-mail: xpguan@sjtu.edu.cn).

Digital Object Identifier 10.1109/TVT.2020.3021478

In [14], each time frame length is adjusted frame by frame to ensure the maximum time slot utilization. Since this strategy needs the estimated number of vehicles, it's hard to realize in highly dynamic vehicle density. In fact, when it comes to large-scale system optimization (e.g., clusters-based system), these protocols are improper since global performance optimization requires a high degree of synergy. Hence, the unified-length time slots are used to achieve the synchronous slot handover in all clusters. To overcome the limitations of the fixed-length slot and guarantee the fairness of resource allocation, this paper proposes a round-robin time scheduling method based on node ID.

The common clustering scheme only uses one of the two parameters, i.e. vehicle's location [7], [15] or speed [16]. However, such an unilateral consideration leads to the shorter sustainability and the worse stability of cluster. Hence, a more reasonable clustering criterion which uses vehicles' geographical information and speeds is adopted in [17], [18]. Since our considered channel model involves path loss and Doppler effect caused by the relative distance and speed between vehicles respectively, the clustering method combining geographical information and speed information is naturally applied to this paper.

As for the previously mentioned global performances (SE and EE), many articles only optimized one of the two indexes [19]–[22]. However, in many practical systems, there is a tradeoff between the SE and EE. Hence, a pricing-based approach [25] is adopted for this SE-EE tradeoff problem, in which a network price is introduced to the total power consumption as the penalty for the achievable sum rates. Besides, the SE or EE maximization problem in these articles only consider the scenarios of single-user interference or simplified interference. In reality, the multiuser interference is unavoidable in multiple adjacent clusters which has a unified time scheduling, especially in high cluster density. Since the multiuser interference management which aims to maximize the system SE or EE by power control is intractable, some solutions are sought in these articles [23]–[25]. In [23], Dinkelbach and branch-and-bound methods are used to give global optimal solutions for both the total EE and individual EE optimization problems. In [24], power control schemes based on Geometric Programming are presented to tackle these nonlinear optimization problems with a system-wide objective (e.g., maximizing the system SE), subject to QoS constraints that is interference-limited. Singh *et al.* [25] resort to lower bound approximation namely successive convex approximation (SCA) along with variable transformation to convert the intractable utility function into a concave one. Compared with Dinkelbach and branch-and-bound methods in [23], SCA method in [24], [25] is also used in this paper due to its lower complexity. The above works are mostly launched in full channel state information (CSI) assumption. For the high-mobility VANETs, wireless channels change more rapidly over time and the full CSI assumption is no longer applicable, which is called as the dilemma of information uncertainty [26]. Besides, optimization with full CSI needs a real-time power control scheme which leads to high computational and communication overhead. Thus, the channel estimation technology based on the feedback CSI and statistical channel tracking error [7] is necessary in the power control designs of vehicular network. To handle the random variables in the channel gain, the interference constraints of all cluster heads (CHs) are cast as probability constraints which are mostly nonconvex and intractable. To obtain the closed forms of these probabilistic constraints and achieve a RPC scheme, convex approximations of probability constraints have been proposed in [27]. Thereinto, Bernstein method has been widely used to tackle random channel fluctuation in [28]–[31]. Based on the characteristics of our constraints, Bernstein method is also used in this paper.

B. Contributions

In this paper, pricing-based RPC schemes involving with imperfect CSI and multiuser interference are proposed to optimize the system SE and EE performances. Unlike the previous unilateral researches on data link layer or physical layer, a highly collaborative system network is investigated and the corresponding effective solution is proposed. The key contributions of this paper are as follows:

- For data link layer, a fixed-length-slot-based protocol with low overhead is proposed to coordinate the system SE/EE of all clusters. Besides, a round-robin time scheduling method based on nodes' orders is proposed to avoid the idle time and guarantee the fairness of resource allocation.
- For physical layer, a clustering scheme based on location and speed is used to improve cluster stability; a mobile stochastic channel model based on vehicles' relative speed is used to describe the impacts of the Doppler effect; and the corresponding RPC schemes are proposed to optimize the system SE/EE. SCA and Bernstein methods are introduced to tackle the non-convex problem with probability constraints. Also, it is the first successful attempt to combine clustering and RPC with velocity parameter to improve the system stability and reliability.
- A general pricing-based framework is leveraged to achieve the maximal SE/EE. In the process of maximizing the pricing-based utility, C-price algorithm and C^*-based EE maximization algorithm are proposed to obtain the optimal solutions.

The rest of the paper is organized as follows: Section II gives the system and channel models, as well as time scheduling strategy. In Section III, formulation and transformations for the pricing-based problem are provided, and the problem is transformed into a standard concave maximization problem. The optimal power control and pricing solutions are developed in Section IV. Then, simulation results and performance analysis are given in Section V. Finally, conclusions are drawn in Section VI.

Notation: In this paper, vectors are typefaced using bold lowercase letters. Some notations are given in Table II.

II. TDMA-Based Multi-Cluster Network

A. Clustering Scheme

The detailed clustering scheme runs through these following two phases.

1) Initial Clustering Stage: The base station (BS) first assigns a node ID to the new vehicle based on the admission order

TABLE I
COMPARISON OF SOLUTIONS-BASED ON ELEMENTS

Related work	clustering scheme		power control scheme	
	location	speed	uncertain CSI	M.I.
Ref.[15]	✓	✗	✗	✗
Ref.[16]	✗	✓	✗	✗
Ref.[19]	✓	✗	✗	✓
Ref.[17],[18]	✓	✓	✗	✗
Ref.[7],[20]	✓	✗	✓	✓
Our work	✓	✓	✓	✓

M.I.: multiuser interference.

TABLE II
NOTATIONS

$\Pr\{\cdot\}$	Probability function.
R^n	Set of n-dimensional real vectors.
$E\{\cdot\}$	Mathematical expectation of a random variable.
$D\{\cdot\}$	Variance of a random variable.
a^T	Transpose of a vector.
$\circ$	Hadamard product of two vectors/matrices.
M	Index set of all time slots $M = \{1, 2, \cdots, M\}$.
I	Index set of all active CMs $I = \{1, 2, \cdots, N\}$.
J	Index set of all CHs $J = \{1, 2, \cdots, N\}$.

of vehicles. After that, all nodes broadcast the Hello packets periodically and build their neighbor lists based on the received Hello packets from other nodes. Note that their node IDs are exchanged when the overtaking operation occurs. Through calculation and comparison, the node having the smallest relative mobility in their neighborhoods is selected as the CH. The adjacent nodes of CH are accepted as cluster members (CM) when they are within CH's effective communication range. Under the received-signal-strength-based (RSS) discriminant criteria combining location and velocity informations, the vehicle having the smaller relative speed difference with CH is more likely to be determined as a CM. To prevent too long service waiting in areas with high node density, the number of CMs is limited to N_U in each cluster.

2) Cluster Maintaining Stage: A short-term connection lost between CM and its CH should be considered. In the fixed-length time slot, there will be a remaining time slot if CM leaves its CH coverage area ahead of schedule, and the time will be used by the next active CM which is candidate for communicating with CH. To maintain the relatively optimal overall performance through the minimum computation, the next active CM's power should be identical with the leaving CM. Besides, if the short-term connection lost between CM and its CH is caused by the channel fluctuations, our proposed RPC is an adequate solution. In this stage, two clusters may also move into each other's coverage area with the movement of nodes. This may lead to the situation where a vehicle has acceptable RSS for more than one CHs (at most two CHs in this paper due to the unidirectional two-lane scene). Since the same direction motion is considered here, the most suitable strategy for CH selection is based on the connection duration. If the CM's velocity isn't equal to that of two CHs,' the CM will join the cluster whose CH is approaching to it. If the CM's velocity is equal to that of two CHs,' the CM will join the cluster which can provide the CM with the higher RSS communication link.

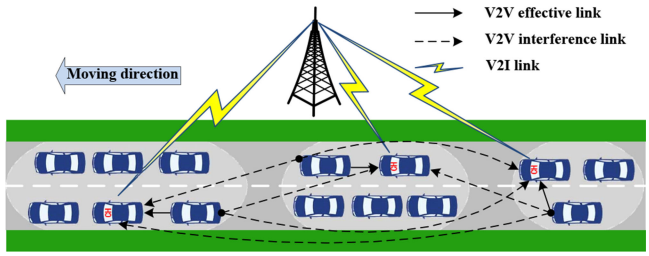

Fig. 1. System model.

B. System Model

In this paper, a cluster-based vehicular network with IEEE 802.11p-LTE hybrid architecture is depicted in Fig. 1. The BS locates on one side of the unidirectional two-lane road, and the road section with three clusters is covered by the communication service region of BS. According to the description of Cowan's M3 model [32], distances between adjacent clusters follow a truncate exponential distribution, then, the vehicles' speeds are assumed to meet the constant speed motion model [33] in every time slot. To ensure that all effective links have high QoS, clusters' boundaries are determined by the minimum RSS requirements. Comparing the measured RSS parameter of CM with the minimum RSS threshold, CH then decides whether to divide the CM into its own cluster or not. In each cluster, there are one CH and several CMs whose total number is uncertain.

Since the cluster system adopts TDMA technology, each CH can only communicate with one CM of its cluster in one time slot, and other CMs of the cluster communicate with their CH sequentially based on the previously allocated time sequence. Given all clusters use the same time scheduling strategy, their effective links coexist and are synchronously switched on any one time slot. The vehicles possess two interfaces: IEEE 802.11p and LTE. CMs can only communicate with their CH via IEEE 802.11p, while CHs communicate with both their CMs via IEEE 802.11p and the BS via LTE. The reference time scale of the packet transmission is of milliseconds. Assume the variation of the vehicles' speed is negligible within the reference time interval, and all signals from the transmitters to the receivers are transmitted through the line of sight (LOS) propagation.

C. Time Scheduling Strategy

When the new vehicle enters the coverage area of BS, it's registered to the BS by the LTE cellular network, and then the vehicle receives some broadcast commands from the BS. These commands require the vehicle to broadcast the Hello packets periodically and build their neighbor lists. Besides, the newly joined vehicle's time needs to be calibrated to ensure the identical time slot switching in all clusters. Once the CH is determined, the status informations of its adjacent vehicles will be evaluated. If the RSS from its adjacent vehicle is qualified, it will join the cluster. And the newly expanded time slot with final order is allocated to the new vehicle by its CH, the orders of these vehicles located behind the departure vehicle move the whole forward one in the next schedule. For clarity, Fig. 2 shows three types of time periods (i.e., transmission period,

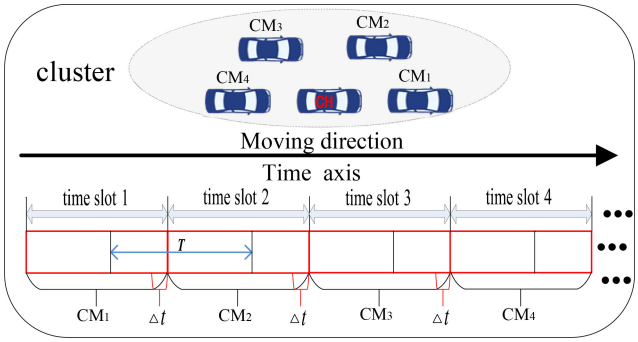

Fig. 2. TDMA slots scheduling principle.

scheduling period and CSI feedback period) on the time axis. The transmission periods are these fixed-length time slots which are alternately allocated to CM_1-CM_4 based on their ID order; The short scheduling period Δt overlapping at the end of each CM's transmission period is used for collecting and handling the latest status informations of all vehicles in the cluster, and then the CH makes a new time scheduling; The fixed CSI feedback period T is also smaller than transmission period and this CSI feedback from the active CM to its CH provides delayed and less precise CSIs due to signal demodulation and vehicle mobility.

D. Channel Model

The system channel model is mainly mobile V2V channel model. Due to the fast mobility of vehicles, their CSIs are hard to be estimated precisely. The CSI of mobile links are reported to CH periodically with corresponding period T. Considering the effects of vehicle's velocity on channel gain, the first-order Gauss-Markov process [34], [35] is used to model the channel fast fading component over the corresponding time slot

$$h = \varpi \hat{h} + e, \tag{1}$$

where h and $\hat{h}$ denote the mobile links' channel fast fading component in the current and previous time respectively. The coefficient ϖ $(0 \leq \varpi < 1)$ quantifies channel correlation between the two consecutive time intervals, and e is the channel discrepancy term distributed according to $\mathcal{CN}(0, 1-\varpi^2)$ and independent of $\hat{h}$. For the Jakes' statistical model [34], ϖ is formulated by $\varpi = J_0(2\pi f_D T)$, where $J_0(\cdot)$ is the zero-order Bessel function. And $f_D = |\Delta v| f_c / c$ refers to the maximum Doppler frequency with $c = 3 \times 10^8$ m/s. f_c is the carrier frequency at 5.9 GHz, and $|\Delta v|$ is the relative vehicle speed.

As a result, the mobile V2V channel power gain of the effective links and interference links in mth time slot can be expressed as a shared expression:

$$G_{ij}^m = H_{ij}^m((\varpi_{ij}^m \hat{h}_{ij}^m)^2 + |e_{ij}^m|^2), i \in \mathcal{I}, j \in \mathcal{J}, m \in \mathcal{M}, \tag{2}$$

where H_{ij}^m denotes the mth time slot large-scale fading effects including shadow-fading and path loss from ith transmitter to jth receiver on the road section. And (2) is composed of the large-scale fading H_{ij}^m and the small-scale fast fading component (1).

By defining $\hat{g}_{ij}^m = H_{ij}^m(\varpi_{ij}^m \hat{h}_{ij}^m)^2$, and $\tilde{g}_{ij}^m = H_{ij}^m |e_{ij}^m|^2$, (2) is equivalent to the following expression

$$G_{ij}^m = \hat{g}_{ij}^m + \tilde{g}_{ij}^m, \quad i \in \mathcal{I}, j \in \mathcal{J}, m \in \mathcal{M}, \tag{3}$$

where G_{ij}^m is the mth time slot interference channel gain from the ith CM transmitter to jth cluster's CH receiver when $i \neq j$, G_{ii}^m represents the effective channel gain of the ith cluster when $j = i$. Moreover, $\hat{g}_{ij}^m$ and $\tilde{g}_{ij}^m$ represent the captured channel gain in previous time and channel error gain among these clusters, respectively. $\hat{g}_{ij}^m$ is an observed value. $\tilde{g}_{ij}^m$ denotes an exponential random variable with parameter $\frac{1}{H_{ij}^m(1-\varpi_{ij}^{m^2})}$.

Since all effective communication links of these clusters are synchronously switched, the resource allocations of the newly configured links can be distributedly realized. The power control problem over the whole time period can be simplified as a power control problem in a general time slot.

Hence, the interference channel gain matrix of N clusters in an arbitrary time slot can be represented as

$$\mathbf{I} = (\mathbf{G}_1, \ldots, \mathbf{G}_j, \ldots, \mathbf{G}_N)_{N \times N}, \tag{4}$$

where $\mathbf{G}_j = (G_{1j}, \ldots, G_{j-1,j}, 0, G_{j+1,j}, \ldots, G_{Nj})^T, \forall j \in \mathcal{J}$; $\mathbf{G}_j = \hat{\boldsymbol{g}}_j + \tilde{\boldsymbol{g}}_j$ with $\hat{\boldsymbol{g}}_j = (\hat{g}_{1j}, \ldots, \hat{g}_{j-1,j}, 0, \hat{g}_{j+1,j}, \ldots, \hat{g}_{Nj})^T$ and $\tilde{\boldsymbol{g}}_j = (\tilde{g}_{1j}, \ldots, \tilde{g}_{j-1,j}, 0, \tilde{g}_{j+1,j}, \ldots, \tilde{g}_{Nj})^T$.

The Signal to Interference plus Noise Ratio (SINR) at the jth cluster's CH from its active CM in the shared time slot can be written as

$$\gamma_j(\mathbf{p}) = \frac{G_{jj} p_j}{\mathbf{G}_j^T \mathbf{p} + \delta^2}, \tag{5}$$

where p_j denotes the transmit power of the active CM in jth cluster, and $\mathbf{p} = [p_1, \ldots, p_j, \ldots, p_N]$ is the vector of all active CMs' transmit powers, $\mathbf{G}_j$ denotes the interference channel gain vector from other clusters' CM transmitters to jth cluster's CH receiver, δ^2 is the noise power.

III. Formulation and Transformations for the Pricing-Based Problem

A. Pricing-Based RPC Problem

In the general time slot, the interference constraint of each cluster's effective link can be posed as a probability constraint since the mobile channel is rapidly changing and contains the random estimated error; and the real-time SINR $\gamma(\mathbf{p})$ in objective function is replaced by the average SINR $\bar{\gamma}(\mathbf{p})$ in larger time scales [7], which is also called long term SINR. Besides, a network price $C \geq 0$ of consuming power resource is defined for a good balance between the long term sum rates and the consuming power in the objective of (6). So, the pricing-based RPC problem is formulated as

$$\begin{aligned} \max_{\mathbf{p}} \; & U(\mathbf{p}) = \sum_{i=1}^{N} \log_2(1 + \bar{\gamma}_i(\mathbf{p})) - C\left(\sum_{i=1}^{N} \zeta_i p_i + P_C\right) \\ \text{s.t.} \; & \begin{cases} \Pr\{\mathbf{G}_j^T \mathbf{p} \leq I_{th}\} \geq 1 - \varepsilon, & j \in \mathcal{J}, \\ 0 \leq p_i \leq p_{i,\max}, & i \in \mathcal{I}, \end{cases} \end{aligned} \tag{6}$$

where $U(\mathbf{p})$ denotes the network utility of EE or SE which depends on the network price, C. The co-channel bandwidth is normalized as 1. $\bar{\gamma}_i(\mathbf{p})$ is the long term SINR of the ith cluster's effective link, and $\zeta_i > 1$ represents the amplifier coefficient for the active CM in ith cluster. $p_{i,\max}$ is the maximum transmit power of the active CM in ith cluster, P_C denotes the circuit power consumption of all active CMs in the involved time slot. I_{th} is all CHs' maximal tolerable interference threshold, and these probabilistic constraints in (6) describe that the total interference of each CH caused by other clusters' active CMs shouldn't exceed I_{th} in the vast majority of cases.

Remark 1: When $C \to 0$, it implies that the cost of the consuming power is almost zero, and the problem (6) degenerates into a sum rate maximization problem. With the increase of the price, the network utility turns into an EE-like optimization objective. Especially, there are no good power allocation policy to optimize the network utility when $C \to \infty$.

B. Uncertainty Transformation in Probability Constraint

In reality, the fluctuant range of the channel error gain is finite and more in line with truncated exponential distribution due to the severe channel fading environment and A/D converters. Based on this type of channel uncertainty, these probability constraints in (6) are nonconvex and intractable. Hence, an appropriate convex approximation method namely Bernstein approximation [27], [36] is introduced.

Definition 1: $\mathbf{p}$ is a deterministic parameter vector, and $\{\eta_n\}$ are random variables with marginal distributions denoted as $\{\xi_n\}$. The following probability constraint (7)

$$Pr\left\{ f_0(\mathbf{p}) + \sum_{n=1}^{N} \eta_n f_n(\mathbf{p}) \le 0 \right\} \ge 1 - \varepsilon, \tag{7}$$

can be replaced by the following conservative approximation

$$\inf_{\rho>0} \left[f_0(\mathbf{p}) + \rho \sum_{n=1}^{N} \Omega_n(\rho^{-1} f_n(\mathbf{p})) + \rho \ln\left(\frac{1}{\varepsilon}\right) \right] \le 0, \tag{8}$$

which is under the following assumptions:

1) $\{f_n(\mathbf{p})\}$ are affine in $\mathbf{p}$, $\forall n = 1, 2, \ldots, N$.

2) $\{\eta_n\}$ satisfy a given distribution family and are independent of each other.

3) $\{\xi_n\}$ have a common bounded support of $[-1, 1]$, that is $-1 \le \xi_n \le 1, \forall n = 1, 2, \ldots, N$.

where $\Omega_n(y) = \max_{\xi_n} \ln(\int \exp(xy) d\xi_n(x))$ in (8). If $\Omega_n(y)$ could be calculated efficiently, the Bernstein method has a good convex approximation of (7). Furthermore, $\Omega_n(y)$ in (8) can be substituted by the following upper bound

$$\Omega_n(y) \le \max\{\mu_n^- y, \mu_n^+ y\} + \frac{\sigma_n^2}{2} y^2, n = 1, \ldots, N, \tag{9}$$

where μ_n^-, μ_n^+ with $-1 \le \mu_n^- \le \mu_n^+ \le 1$ and $\sigma_n \ge 0$ are constants that depend on the given families of probability distributions.

Substituting $\Omega_n(\cdot)$ in (8) with this upper bound and using the arithmetic-geometric inequality, the inequality (8) can be further formulated as,

$$f_0(\mathbf{p}) + \sum_{n=1}^{N} \max\{\mu_n^- f_n(\mathbf{p}), \mu_n^+ f_n(\mathbf{p})\} + \sqrt{2\ln\left(\frac{1}{\varepsilon}\right)} \left(\sum_{n=1}^{N} \sigma_n^2 f_n(\mathbf{p})^2 \right)^{\frac{1}{2}} \le 0, \tag{10}$$

which is a convex conservative surrogate for (7).

Remark 2: In general, the values of these parameters (i.e., μ_n^-, μ_n^+ and σ_n) can be directly captured in the Table I of *[36]*. However, such parameters for truncated exponential distribution aren't immediately available in this table. Hence, additional calculation process for solving the parameters are given in Appendix A.

Suppose that the truncated distributions of $\{\tilde{g}_{ij}\}(i \ne j)$ have bounded supports $[a_{ij}, b_{ij}]$. Introduce constants $\alpha_{ij} = \frac{1}{2}(b_{ij} - a_{ij}) \ne 0$ and $\beta_{ij} = \frac{1}{2}(b_{ij} + a_{ij})$ to normalize the supports to $[-1, 1]$ as follows,

$$\xi_{ij} = \frac{\tilde{g}_{ij} - \beta_{ij}}{\alpha_{ij}} \in [-1, 1], \tag{11}$$

where $\boldsymbol{\alpha}_j = [\alpha_{1j}, \ldots, \alpha_{j-1,j}, 0, \alpha_{j+1,j}, \ldots, \alpha_{Nj}]^T$, $\boldsymbol{\beta}_j = [\beta_{1j}, \ldots, \beta_{j-1,j}, 0, \beta_{j+1,j}, \ldots, \beta_{Nj}]^T$.

Let $f_{0j}(\mathbf{p}) = -I_{th} + \sum_{i=1, i\ne j}^{N} (\hat{g}_{ij} + \beta_{ij}) p_i$ and $f_{ij}(\mathbf{p}) = \alpha_{ij} p_i$ for $i \in \mathcal{I}$, $j \in \mathcal{J}$, all probability constraints in (6) are equivalent to (7). Replacing $f_{0j}(\mathbf{p})$ and $f_{ij}(\mathbf{p})$ into (10), we can obtain

$$-I_{th} + \sum_{i\ne j}^{N} (\hat{g}_{ij} + \beta_{ij}) p_i + \sum_{i\ne j}^{N} \mu_{ij}^+ \alpha_{ij} p_i + \sqrt{2\ln\left(\frac{1}{\varepsilon}\right)} \left(\sum_{i\ne j}^{N} (\sigma_{ij}\alpha_{ij} p_i)^2 \right)^{\frac{1}{2}} \le 0, j \in \mathcal{J}, \tag{12}$$

where $\boldsymbol{\mu}_j^+ = [\mu_{1j}^+, \ldots, \mu_{j-1,j}^+, 0, \mu_{j+1,j}^+, \ldots, \mu_{Nj}^+]^T$, $\boldsymbol{\sigma}_j = [\sigma_{1j}, \ldots, \sigma_{j-1,j}, 0, \sigma_{j+1,j}, \ldots, \sigma_{Nj}]^T$.

The variables p_i are nonlinearly coupled in the last term of (12), and the complexity of searching for the optimal $\mathbf{p}$ increases rapidly as N grows. To relieve this issue, the last term in (12) containing ℓ_2-norm of the vector $\mathbf{z} = [\sigma_{1j}\alpha_{1j}p_1, \ldots, \sigma_{j-1,j}\alpha_{j-1,j}p_{j-1}, 0, \sigma_{j+1,j}\alpha_{j+1,j}p_{j+1}, \ldots, \sigma_{Nj}\alpha_{Nj}p_N]$ is further approximated by $\|\mathbf{z}\|_2 \le \|\mathbf{z}\|_1$ for any $\mathbf{z} \in \mathbb{R}^N$. Besides, these parameters (i. e., σ_{ij} and α_{ij}) are deduced to be positive in Appendix A. Based on these, the constraint in (12) is further formulated as

$$\sum_{i=1}^{N} \chi_{ij} p_i + \sqrt{2\ln\left(\frac{1}{\varepsilon}\right)} \sum_{i=1}^{N} \sigma_{ij}\alpha_{ij} p_i \le I_{th}, j \in \mathcal{J}, \tag{13}$$

where $\chi_{ij} = \hat{g}_{ij} + \mu_{ij}^+ \alpha_{ij} + \beta_{ij}$.

To pursue a simple form of (13), an operation of two matrices namely Hadamard product [37] is introduced.

Definition 2: Given two matrices $\mathbf{A} = [a_{ij}]$ and $\mathbf{B} = [b_{ij}]$ with the same dimension (not necessarily square), the Hadamard product between $\mathbf{A}$ and $\mathbf{B}$ in a given operational symbol ($\circ$) is

the element-wise product $\mathbf{A} \circ \mathbf{B} \equiv [a_{ij}b_{ij}]$, which has the same dimension as $\mathbf{A}$ and $\mathbf{B}$.

Hence, the inequality in (13) can be rewritten as

$$\boldsymbol{\chi}_j^T \mathbf{p} + \sqrt{2\ln\left(\frac{1}{\varepsilon}\right)}(\boldsymbol{\sigma}_j \circ \boldsymbol{\alpha}_j)^T \mathbf{p} \le I_{th}, j \in \mathcal{J}, \tag{14}$$

where $\boldsymbol{\chi}_j = \hat{\boldsymbol{g}}_j + \boldsymbol{\mu}_j^+ \circ \boldsymbol{\alpha}_j + \boldsymbol{\beta}_j$.

In consequence, the intractable probabilistic constraints in (6) are eventually transformed into the tractable deterministic constraints.

C. Transformation of Nonlinear Objective Function

The nonlinear objective function of (6) is intractable due to the nonconvex long term sum rates about $\mathbf{p}$. As a method with low computational overhead, SCA method is applied to impose a lower bound on the long term sum rates ($R_s(\mathbf{p})$, in bits/s/Hz) for all the N effective intra-cluster links in a general time slot,

$$\begin{aligned} R_s(\mathbf{p}) &= \sum_{i=1}^{N} \log_2(1+\bar{\gamma}_i(\mathbf{p})) \\ &\ge \frac{1}{\ln 2}\sum_{i=1}^{N}\left[X_i \ln(\bar{\gamma}_i(\mathbf{p})) + Y_i\right] \triangleq R_{s,lb}(\mathbf{p}), \end{aligned} \tag{15}$$

where X_i and Y_i are renewed by $X_i = \tau_i/(1+\tau_i)$ and $Y_i = \ln(1+\tau_i) - X_i \ln \tau_i$, $\forall \tau_i > 0$ [38]. In fact, the equality in (15) holds when $X_i = \bar{\gamma}_i(\mathbf{p})/(1+\bar{\gamma}_i(\mathbf{p}))$ and $Y_i = \ln(1+\bar{\gamma}_i(\mathbf{p})) - X_i \ln(\bar{\gamma}_i(\mathbf{p}))$, and the equality is satisfied $(X_i, Y_i) =$(1,0) when $\bar{\gamma}_i(\mathbf{p}) \to \infty$.

Based on (14) and (15), the optimization in (6) can be reformulated as

$$\begin{aligned} &\max_{\mathbf{p}} U_{lb}(\mathbf{p}) = R_{s,lb}(\mathbf{p}) - C\left(\sum_{i=1}^{N}\zeta_i p_i + P_C\right) \\ &\text{s.t.} \begin{cases} \boldsymbol{\chi}_j^T \mathbf{p} + \sqrt{2\ln(\frac{1}{\varepsilon})}(\boldsymbol{\sigma}_j \circ \boldsymbol{\alpha}_j)^T \mathbf{p} \le I_{th}, & j \in \mathcal{J}, \\ 0 \le p_i \le p_{i,\max}, & i \in \mathcal{I}, \end{cases} \end{aligned} \tag{16}$$

where $U_{lb}(\mathbf{p})$ is a tight lower bound of $U(\mathbf{p})$ and is considered to be an equivalent for the utility function $U(\mathbf{p})$.

This optimization in (16) is still nonlinear and intractable with respect to the power vector $\mathbf{p}$. However, when a logarithmic transformation for each element in the power vector $\mathbf{p}$ is performed (i.e., $\tilde{p}_i = \ln p_i$), the transformed problem of (16) can be proved to be a standard concave maximization problem [38]. It is noted that the intersection of all transformed log-domain interference constraints in (17) is still a convex set, and the relevant proof is provided in Appendix B.

IV. Optimal Power Control and Pricing Solutions

In this section, a C-price algorithm is first proposed to provide a general framework for the maximal SE/EE of the vehicular network. The maximal SE can be obtained directly when $C \to 0$ is deployed in this algorithm. However, the maximum EE at the optimal price C^* isn't directly available since the optimal price C^* needs an additional procedure to solve. Hence, the EE maximization algorithm which based on the C-price algorithm is further proposed to capture the optimal price C^*, i.e., the maximal EE of the vehicular network.

A. Optimal C-Price Power Control Algorithm

By the logarithmic transformation of power vector, the formula in (16) is transformed as follows,

$$\begin{aligned} &\max_{\tilde{\mathbf{p}}} U_{lb}(\mathrm{e}^{\tilde{\mathbf{p}}}) \\ &s.t. \begin{cases} \boldsymbol{\chi}_j^T \mathrm{e}^{\tilde{\mathbf{p}}} + \sqrt{2\ln(\frac{1}{\varepsilon})}(\boldsymbol{\sigma}_j \circ \boldsymbol{\alpha}_j)^T \mathrm{e}^{\tilde{\mathbf{p}}} \le I_{th}, & j \in \mathcal{J}, \\ -\infty \le \tilde{p}_i \le \ln p_{i,\max}, & i \in \mathcal{I}. \end{cases} \end{aligned} \tag{17}$$

To pursue an iterative algorithm for solving the problem (17), Lagrange dual decomposition technique [39] is used to maximize the lower bound of the original objective under given coefficients X_i and Y_i. It's noted that these two coefficients should be updated to guarantee a monotonic increase in the lower bound performance.

Hence, the Lagrangian function of (17) under fixed coefficients X_i and Y_i can be expressed as

$$\begin{aligned} &\mathcal{L}(\tilde{\mathbf{p}}, \boldsymbol{\lambda}) \\ &= U_{lb}(\mathrm{e}^{\tilde{\mathbf{p}}}) - \sum_{j=1}^{N}\lambda_j\left(\boldsymbol{\chi}_j^T \mathrm{e}^{\tilde{\mathbf{p}}} + \sqrt{2\ln\left(\frac{1}{\varepsilon}\right)}(\boldsymbol{\sigma}_j \circ \boldsymbol{\alpha}_j)^T \mathrm{e}^{\tilde{\mathbf{p}}} - I_{th}\right) \\ &= \frac{1}{\ln 2}\sum_{i=1}^{N}\left[X_i \ln(\bar{\gamma}_i(\mathrm{e}^{\tilde{\mathbf{p}}})) + Y_i\right] - C\left(\sum_{i=1}^{N}\zeta_i \mathrm{e}^{\tilde{p}_i} + P_C\right) \\ &\quad - \sum_{j=1}^{N}\lambda_j\left(\boldsymbol{\chi}_j^T \mathrm{e}^{\tilde{\mathbf{p}}} + \sqrt{2\ln\left(\frac{1}{\varepsilon}\right)}(\boldsymbol{\sigma}_j \circ \boldsymbol{\alpha}_j)^T \mathrm{e}^{\tilde{\mathbf{p}}} - I_{th}\right), \end{aligned} \tag{18}$$

where $\boldsymbol{\lambda} = [\lambda_1, \ldots, \lambda_N] \ge \mathbf{0}$ is the Lagrangian multiplier vector for all CHs' interference constraints in (17).

The optimal solution of (17) can be obtained by solving its dual problem, and the ultimate dual problem can be reformulated as

$$\min_{\boldsymbol{\lambda} \ge \mathbf{0}} \max_{\tilde{\mathbf{p}}} \mathcal{L}(\tilde{\mathbf{p}}, \boldsymbol{\lambda}). \tag{19}$$

The dual problem is achieved in an alternate iterative mode which between a subproblem, renewing the log-domain power vector $\tilde{\mathbf{p}}$ by fixing the multiplier vector $\boldsymbol{\lambda}$, and a master problem, updating each multiplier in $\boldsymbol{\lambda}$ according to the allocated log-domain power vector $\tilde{\mathbf{p}}$.

Subproblem Solution: To pursue the corresponding power iteration about $\tilde{p}_i$, the partial derivative of (18) with respect to $\tilde{p}_i$ is forced to equal zero. Based on these, the $(t+1)^{th}$ power iteration is deduced into the following fixed-point iteration,

$$\begin{aligned} \tilde{p}_i^{(t+1)} = \Bigg[&\ln\left(\frac{X_i^{(t)}}{\ln 2}\right) - \ln\left(\frac{1}{\ln 2}\sum_{j\ne i}^{N} X_j^{(t)} \frac{\bar{\gamma}_j^{(t)}(\mathrm{e}^{\tilde{\mathbf{p}}})\overline{G_{ij}}}{\mathrm{e}^{\tilde{p}_j^{(t)}}\overline{G_{jj}}} + C\zeta_i \right. \\ &\left. + \sum_{j\ne i}^{N}\lambda_j^{(t)}\left(\chi_{ij} + \sqrt{2\ln\left(\frac{1}{\varepsilon}\right)}\sigma_{ij}\alpha_{ij}\right)\right)\Bigg]_{-\infty}^{\ln p_{i,\max}}, \end{aligned} \tag{20}$$

Algorithm 1: C-Price Algorithm: RPC Algorithm for Fixed Price.

1: **Input:** Set the maximal iterative number $\mathcal{T}_{\max}$, the fixed price C and the step size ϕ.
2: **Initialization:** Initialize the counter $t=1$, the log-domain power vector $\tilde{\mathbf{p}}$ and the Lagrangian multiplier vector $\boldsymbol{\lambda}$.
3: **repeat**
4: Calculate $\bar{\gamma}_i^{(t)}(\mathrm{e}^{\tilde{\mathbf{p}}})$, $X_i^{(t)} \leftarrow \bar{\gamma}_i^{(t)}(\mathrm{e}^{\tilde{\mathbf{p}}})/(1+\bar{\gamma}_i^{(t)}(\mathrm{e}^{\tilde{\mathbf{p}}}))$ and $Y_i^{(t)} \leftarrow \log_2(1+\bar{\gamma}_i^{(t)}(\mathrm{e}^{\tilde{\mathbf{p}}})) - X_i^{(t)}\log_2(\bar{\gamma}_i^{(t)}(\mathrm{e}^{\tilde{\mathbf{p}}}))$, $\forall i \in \mathcal{I}$.
5: Update $\tilde{\mathbf{p}}$ and $\boldsymbol{\lambda}$ using (20) and (23), respectively.
6: Set $t \leftarrow t+1$.
7: **until** $\tilde{\mathbf{p}}$, $\boldsymbol{\lambda}$ synchronously converge to the optimal solutions $\tilde{\mathbf{p}}^*$, $\boldsymbol{\lambda}^*$ or $t > \mathcal{T}_{\max}$.
8: **Output:** $\mathrm{e}^{\tilde{\mathbf{p}}^*}$.

where $[x]_a^b = \min\{\max\{x,a\},b\}$, $\overline{G_{ij}}$ and $\overline{G_{jj}}$ are the mean values of G_{ij} and G_{jj} in the time slot, respectively. $\overline{G_{ij}} = \mathbb{E}\{G_{ij}\} = \hat{g}_{ij} + \bar{g}_{ij}$ with $\mathbb{E}\{\hat{g}_{ij}\} = \hat{g}_{ij}$ and $\mathbb{E}\{\tilde{g}_{ij}\} = \bar{g}_{ij}$; $\overline{G_{jj}} = \mathbb{E}\{G_{jj}\} = \hat{g}_{jj} + \bar{g}_{jj}$ with $\mathbb{E}\{\hat{g}_{jj}\} = \hat{g}_{jj}$ and $\mathbb{E}\{\tilde{g}_{jj}\} = \bar{g}_{jj}$. Besides, $X_j^{(t)} = \bar{\gamma}_j^{(t)}(\mathrm{e}^{\tilde{\mathbf{p}}})/(1+\bar{\gamma}_j^{(t)}(\mathrm{e}^{\tilde{\mathbf{p}}}))$. Specifically, the long term SINR of the jth cluster's effective link, $\bar{\gamma}_j(\mathrm{e}^{\tilde{\mathbf{p}}})$, can be updated by

$$\bar{\gamma}_j^{(t)}(\mathrm{e}^{\tilde{\mathbf{p}}}) = \frac{\overline{G_{jj}}\mathrm{e}^{\tilde{p}_j^{(t)}}}{\sum_{i=1,i\neq j}^{N}\overline{G_{ij}}\mathrm{e}^{\tilde{p}_i^{(t)}} + \delta^2}. \tag{21}$$

Remark 3: According to the method which combines measurement and message-passing in *[38]*, the log-domain power iteration in (20) can be regarded as a distributed power iteration. Moreover, the type of standard interference function in *[40]* can demonstrate the convergence of this power iteration.

*Master Problem Solution:*According to (18), we can obtain the partial derivative of Lagrangian function with respect to λ_j, namely,

$$\frac{\partial \mathcal{L}(\tilde{\mathbf{p}},\boldsymbol{\lambda})}{\partial \lambda_j} = -\left(\left(\boldsymbol{\chi}_j + \sqrt{2\ln\left(\frac{1}{\varepsilon}\right)}\boldsymbol{\sigma}_j \circ \boldsymbol{\alpha}_j\right)^T \mathrm{e}^{\tilde{\mathbf{p}}} - I_{th}\right). \tag{22}$$

Based on (22), the updating procedure of $\boldsymbol{\lambda}$ using the sub-gradient method are depicted as follows,

$$\lambda_j^{(t+1)} = \left[\lambda_j^{(t)} + \phi_j\left(\left(\boldsymbol{\chi}_j + \sqrt{2\ln\left(\frac{1}{\varepsilon}\right)}\boldsymbol{\sigma}_j \circ \boldsymbol{\alpha}_j\right)^T \mathrm{e}^{\tilde{\mathbf{p}}} - I_{th}\right)\right]^+, \tag{23}$$

where $[x]^+ = \max[0,x]$, and ϕ_j is a positive step-size which decreases with the iterative number t.

The distributed iterative algorithm for the C-price-based RPC problem is summarized in the following Algorithm 1:

Remark 4: Algorithm 1 contains a loop whose time complexity is described by the maximal loop count, $\mathcal{T}_{\max}$. Since there are N clusters which use their power iterations for power optimization, the computational complexity of the Algorithm 1 is $O(N\mathcal{T}_{\max})$. Since the Algorithm 1 are used for the inner loop of Algorithm 2, the computational complexity of the Algorithm 2 is $O(KN\mathcal{T}_{\max})$, where K is the maximum number of outer loop.

The communication overhead is defined as the times of message exchange in each updating period. For the selected algorithm, $2N+1$ message exchanges are required to achieve the optimal power allocation. When it's the turn of the N candidate CMs to communicate with their CHs, they send their CHs messages containing some status informations and all measured channel gains (N messages). Then, the N CHs relay their captured channel gain informations to the central processor located at BS (N messages). Based on these channel gains and the first-order Gauss-Markov process, the central processor executes the selected algorithm, and announces the power allocation decision to all CMs (one message).

B. Optimal Price C^* for Energy Efficiency Maximization

As mentioned earlier, there is a tradeoff between the SE and the EE by adjusting the network price C. When the fixed price C is set as zero, the Algorithm 1 aims to maximize the SE of the whole vehicular network. With the price increasing from zero to infinity, an optimal price C^* inevitably exists to achieve the EE maximization of this network.

More specifically, the system EE ($\eta_{EE}(\mathrm{e}^{\tilde{\mathbf{p}}})$, in bits/Hz/Joule) is defined as the ratio of the achievable long term sum rates to the total power consumptions:

$$\eta_{EE}(\mathrm{e}^{\tilde{\mathbf{p}}}) = \frac{R_s(\mathrm{e}^{\tilde{\mathbf{p}}})}{\sum_{i=1}^{N}\zeta_i\mathrm{e}^{\tilde{p}_i} + P_C} = \frac{\sum_{i=1}^{N}\log_2(1+\bar{\gamma}_i(\mathrm{e}^{\tilde{\mathbf{p}}}))}{\sum_{i=1}^{N}\zeta_i\mathrm{e}^{\tilde{p}_i} + P_C}. \tag{24}$$

Theorem 1: The price C^* is the optimal network price, if and only if the optimal log-domain power solution $\tilde{\mathbf{p}}^*$ in the utility function $U(\mathrm{e}^{\tilde{\mathbf{p}}^*})$ with respect to C^* satisfies the following equilibrium equation:[1]

$$U(\mathrm{e}^{\tilde{\mathbf{p}}^*}) = R_s(\mathrm{e}^{\tilde{\mathbf{p}}^*}) - C^*\left(\sum_{i=1}^{N}\zeta_i\mathrm{e}^{\tilde{p}_i^*} + P_C\right) = 0. \tag{25}$$

Proof: See Appendix C ■

In reality, the maximal EE can't be achieved at the optimal price $C^*=0$ since the transmit power of user must exist. To achieve the EE maximization, the following theorem is given to illustrate the iterative process for the optimal price C^*.

Theorem 2: Define $\tilde{\mathbf{p}}^*(k)$ as the k^{th} iteration local optimal solution of the utility function $U(\mathrm{e}^{\tilde{\mathbf{p}}})$ at the network price $C(k)$. If the $(k+1)^{th}$ price is updated by

$$C(k+1) = \frac{R_s(\mathrm{e}^{\tilde{\mathbf{p}}^*(k)})}{\sum_{i=1}^{N}\zeta_i\mathrm{e}^{\tilde{p}_i^*(k)} + P_C}, \tag{26}$$

then $C(k)$ is monotonically increasing with respect to the iterative number k until the price converges at $C(l), (l \geq k)$. And the optimal price $C^* = \lim_{l\to\infty}C(l)$ satisfies the equilibrium equation (25).

[1]Since the the utility function $U(\mathrm{e}^{\tilde{\mathbf{p}}})$ is non-convex with respect to $\tilde{\mathbf{p}}$, the optimal power solution here is referred to as a local maximizer.

TABLE III
SYSTEM PARAMETERS

Parameter	Value
Carrier frequency (f_c)	5.9 GHz
Cluster effective communication radius (R)	15 m
Radio Range (R_a)	300 m
CSI feedback period of vehicle (T)	1 ms
Average speed of vehicle	25 m/s
Mean of background noise (δ^2)	-30 dBm
Maximum CM transmitter power ($p_{i,max}$)	0.05 W
Log-normal shadowing standard deviation	10 dB
Pathloss model	$d^{-\theta}$, d in m
Pathloss exponent (θ)	3

TABLE IV
RELATIVE VELOCITY $|\Delta v|$ FOR ALL V2V LINKS AT A CERTAIN TIME SLOT

Item	$\lvert\Delta v\rvert$ ($\mathbf{R}^a$ / $\mathbf{T}^a$)	CH_1 (20m/s)	CH_2 (27m/s)	CH_3 (22m/s)	CH_4 (26m/s)	CH_5 (29m/s)
V2V	CM_1(26m/s)	6m/s	1m/s	4m/s	0m/s	3m/s
	CM_2(20m/s)	0m/s	7m/s	2m/s	6m/s	9m/s
	CM_3(28m/s)	8m/s	1m/s	6m/s	2m/s	1m/s
	CM_4(30m/s)	10m/s	3m/s	8m/s	4m/s	1m/s
	CM_5(20m/s)	0m/s	7m/s	2m/s	6m/s	9m/s

[a] $\mathbf{R}$: Receiver. $\mathbf{T}$: Transmitter.

Algorithm 2: EE Maximization Algorithm: RPC Algorithm for C^*-Based EE Maximization.

1: **Input:** Set convergence tolerance ϵ.
2: **Initialization:** Initialize the counter k =1 and the network price $C(1) = 0.1$.
3: **repeat**
4: Find $\tilde{\mathbf{p}}^*(k)$ from Algorithm 1 when $C = C(k)$.
5: Update $C(k+1)$ using (26).
6: Set $k \leftarrow k+1$.
7: **until** $|C(k+1) - C(k)| \leq \epsilon$.
8: **Output:** $e^{\tilde{\mathbf{p}}^*}$, C^*.

Proof: See Appendix D ■

The corresponding algorithm for the optimal-price (C^*)-based EE maximization is proposed as Algorithm 2.

V. SIMULATION RESULTS AND PERFORMANCE ANALYSIS

In this section, numerical simulations are presented to evaluate the performance of the proposed Algorithms 1 and 2. A cluster-based vehicular network system which includes five clusters under a certain time slot is selected as our fundamental simulation scenario. The major system parameters are listed in Table III. Since the influence of vehicle velocities on the channel is concerned, all vehicle velocities and the relative velocities of all V2V links are provided in Table IV. Unless stated otherwise, the parameter value of I_{th} is set to 10^{-6}, the outage probability threshold is $\varepsilon = 0.1$.

Fig. 3(a) and Fig. 3(b) show that the power and the corresponding multiplier convergence performances of each CM transmitter in Algorithm 2, respectively. In fact, these two graphs (i.e., the fixed price $C = C^*$ in Algorithm 1) also illustrate the Algorithm 1 has a quick convergence performance since the power and the corresponding multiplier are synchronously converged at the $4th$ iteration. These phenomenons in Fig. 3

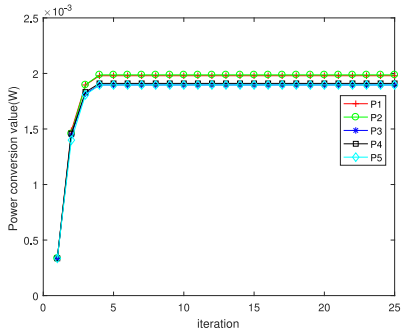

(a)

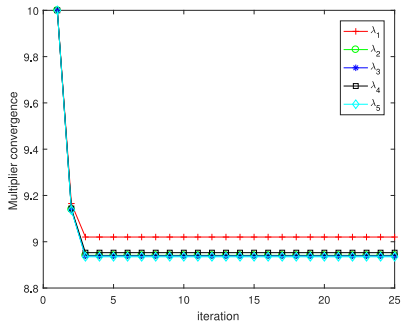

(b)

Fig. 3. Convergence performances of the proposed algorithms. (a) Power convergence performance. (b) Multiplier convergence performance.

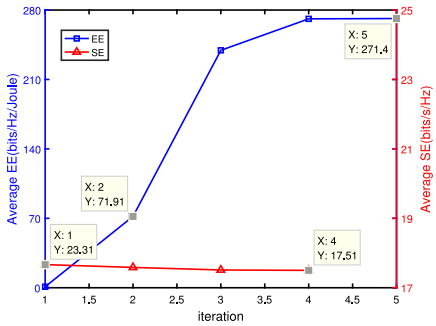

Fig. 4. Average EE and SE performances of Algorithm 2.

demonstrate that the proposed two algorithms can converge to an equilibrium. Furthermore, Fig. 4 shows that the investigated indexes (average EE and SE in a time slot) eventually achieve steady-state performance in the iterative Algorithm 2. More specifically, it's obvious that the systematic average EE (η_{EE}) is monotonically increasing with respect to the iterative number in Fig. 4. This phenomenon also confirms the conclusion of Theorem 2. Besides, the average SE of this system decreases with the increase of the network price C (i.e., the average EE). In the process of pursuing the maximum energy efficiency, the dynamic power consumption $\sum_{i=1}^{N} \zeta_i p_i$ should be decreased with the increase of price C, especially considering that their achieved sum rates are less than the maximal spectral efficiency (C =0). When the power level of users is relatively reduced, the background noise δ^2 in SINR expression is relatively improved, and finally leads to a smaller sum rates. This explains why the

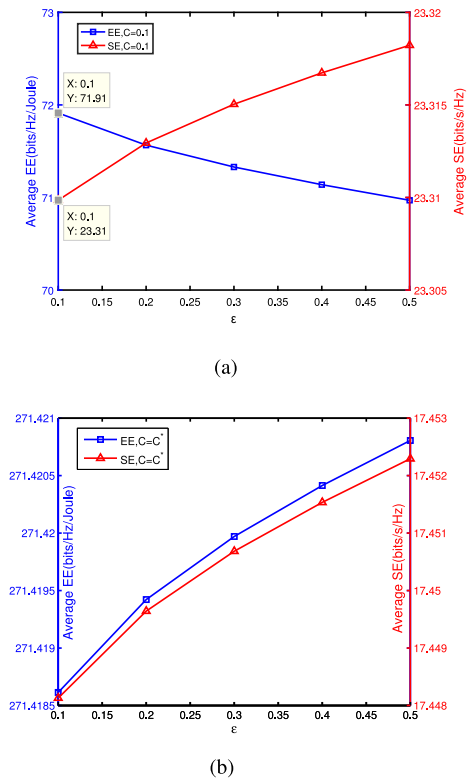

Fig. 5. Average EE and SE versus ε under imperfect CSI. (a) Average EE and SE performance when $C = 0.1$. (b) Average EE and SE performance when $C = C^*$.

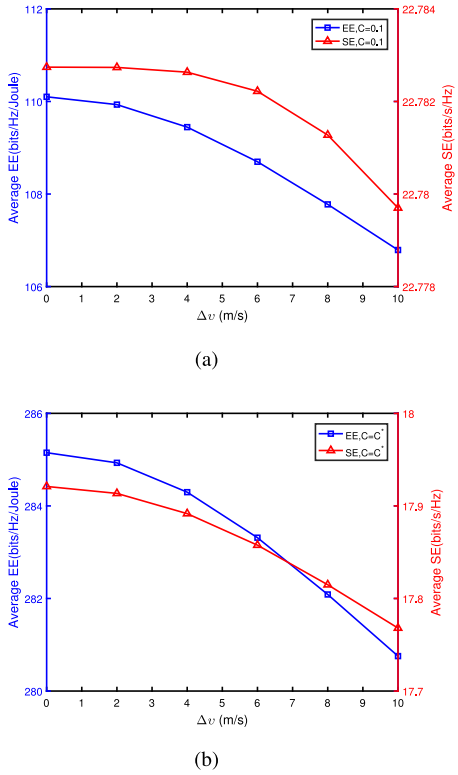

Fig. 6. Average EE and SE versus $\Delta\upsilon$ when $\varepsilon = 0.1$. (a) Average EE and SE versus $\Delta\upsilon$ when $C = 0.1$. (b) Average EE and SE versus $\Delta\upsilon$ when $C = C^*$.

average SE of this system decreases with the increase of the network price C.

To evaluate the performance of the proposed method, Fig. 5 shows the trends of the average EE and SE to ε when the network price $C = 0.1$ (i.e., average SE maximization) and $C = C^*$ (i.e., average EE maximization) under the imperfect CSI. More specifically, Fig. 5(a) shows that the average EE decreases as ε increases, while the average SE has a positive proportional relationship with ε. This phenomenon is reasonable due to the definition of η_{EE} in (24). The average SE R_s, as the numerator of η_{EE}, increases logarithmically as the power vector $\mathbf{p}$ increases, while the denominator of η_{EE} increases linearly with the increase of power vector $\mathbf{p}$. Based on these, the numerator of η_{EE} has a slower growth than the denominator when the power vector grows. In general, greater ε brings higher power levels at transmitters. Hence, the average EE shows an inverse proportional relation with ε. Besides, Fig. 5(b) shows that the average SE and EE share the same growth trend with respect to ε. This phenomenon can be illustrated by Theorem 1. When the average EE at C^* and the transmission powers increase simultaneously with ε, the average SE R_s is inevitably increased to make the equation (25) hold. Compared with Fig. 5(a), both the average SE and EE in Fig. 5(b) have smaller changes with ε. These results illustrate that the double-loop iterative algorithm (Algorithm 2) shows more stable performances than the single-loop iterative algorithm (Algorithm 1) on the average SE and EE.

To further illustrate the impacts of Doppler shift on the involved system performances, different relative vehicle speeds are simulated in the system. In this simulation, the speeds of all CHs are identical (i.e., 20 m/s) and the speeds of all CMs are concurrently increased from 20 to 30 m/s in the same network topologies. This configuration leads to a fact that all active V2V links are involved with Doppler effects. Fig. 6 shows that the Doppler effect caused by the relative speed has a bad impact on both the maximal average SE (i.e., C =0.1) and the maximal average EE (i.e., $C = C^*$). More concretely, Fig. 6(a) shows that the average SE at C =0.1 decreases when the relative speeds of all V2V links increase from 0 to 10 m/s, so does the corresponding average EE of the system. Besides, Fig. 6(b) shows that the average SE/EE at $C = C^*$ have the identical downward trends with the increasing relative speeds of all V2V links. What's more, these results in Fig. 6 also demonstrate the proposed clustering method which prefers to the smaller relative speed is effective.

To verify the robustness of our proposed method, the real outage comparisons under imperfect and perfect CSI are provided in Fig. 7 and Fig. 8. It is worth mentioning that our method is used for the case with imperfect CSI, and the similar method which handles problems with perfect CSI in [25] is dedicated to the perfect CSI case. In these simulations, the real outage percentage (ROP) of all cases are captured by performing 10^4 Monte Carlo experiments, and the random parts in the simulated channel contain two components: shadowing fading with log-normal distribution and fast fading with Rayleigh fading. Whether perfect or imperfect CSI, each case is divided into two broad

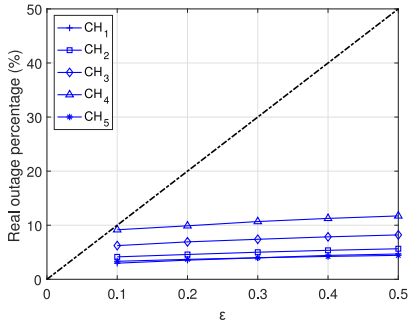

(a)

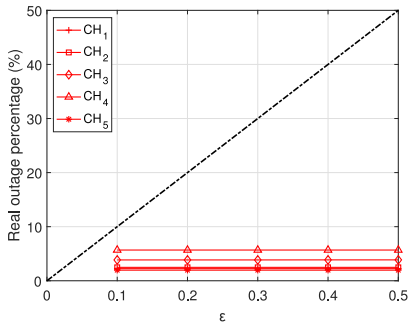

(b)

Fig. 7. Real outage comparison under imperfect CSI. (a) Real outage percentage when $C = 0.1$. (b) Real outage percentage when $C = C^*$.

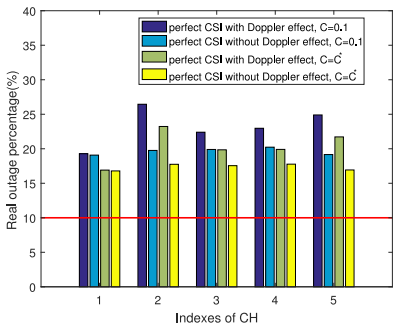

Fig. 8. Real outage comparison under perfect CSI.

categories (i.e., C =0.1 and $C = C^*$) for discussion. In Fig. 7, the legend entries with CH_1-CH_5 denotes the corresponding effective links which is connected with CH_1-CH_5. And so do the indexes of CH in Fig. 8. Fig. 7 shows that all solid lines of ROP in the two subgraphs are below the black dotted lines which stand for the growing outage probability threshold ε. These results demonstrate that the system using our method has well-functioning robustness to resist the channel intrinsic fading and Doppler effect. In detail, that Fig. 7(b) shows the stronger conservatism than Fig. 7(a) illustrates the robustness of Algorithm 2 is better than that of Algorithm 1. Besides, Fig. 8 shows that the ROPs of all effective links involving with perfect CSI are well above the red solid top-line of the ROPs at 10%. Compared with the two subgraphs in Fig. 7, Fig. 8 behaves that the network system which is optimized by the method in [25] are easily interrupted and disfunctional since the ROPs in Fig. 8 are significantly higher than those in Fig. 7. Moreover, Fig. 8

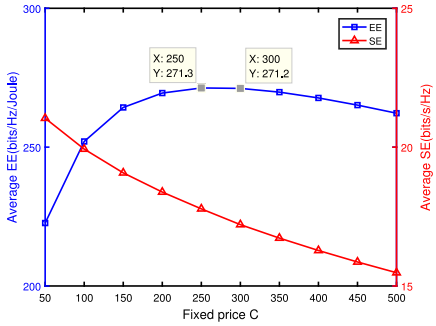

Fig. 9. Average EE and SE for different network prices C.

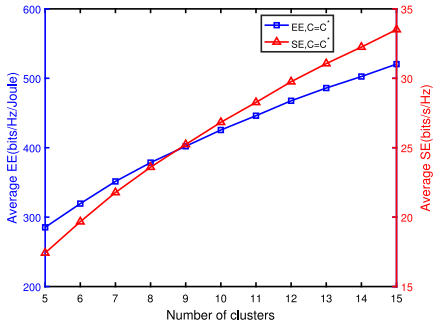

Fig. 10. Average EE and SE versus number of clusters.

reveals that the ROPs of these effective links with Doppler effect are higher than the links without Doppler effect no matter what the value of C is. This phenomenon also demonstrates that the impacts of Doppler effect on the system are detrimental in terms of the effective link's ROP. However, these results in Fig. 7 are still qualified after taking into account the Doppler effect. Based on these, our proposed RPC schemes are effective.

Fig. 9 depicts the impact of different network price C on the tradeoff between the average EE and SE for Algorithm 1. It is clear that the average SE decreases with the growth of the price C, while there exists an optimal price in terms of the maximum average EE at $C = 271.4$. The average EE at the price $C = 250$ or $C = 300$ isn't the the maximum average EE since it isn't equal to fixed price C. Hence, the adjustment of the price C is crucial when there is a tradeoff between the average SE and EE.

To illustrate the impact of vehicle density on the average EE and SE, the number of clusters varies from 5 to 15 in the simulated scenario. Moreover, the speeds of all CHs are set as 20 m/s and the speeds of all CMs are set as 25 m/s. The purpose of setting the same speed is to achieve a more effective comparison. For simplicity, only one circumstance (i.e., the price $C = C^*$) is involved. In Fig. 10, both the average EE and SE increase as the number of clusters increases. However, the growth rates of the two curves are declining. These results indicate that the increasing aggregated interference level caused by the increasing vehicle density leads to the decreasing growth rates of the average EE and SE performances, even if the number of the effective communication links are mounting. Thus, a reasonable maximal cluster size should be set to make each user have a relatively high performance when the vehicle density is high.

Note that some representative programs are given through Github on https://github.com/Xieyuanai/Energy-Spectral-Efficiency-Optimization/. When referring to these codes, please quote clearly in the publications.

VI. Conclusion

In this paper, we have proposed the RPC schemes to achieve the desired performance in the high mobility network. A pricing-based utility was used to balance the power consumption and the sum rate. Moreover, clustering and interference probability constraints were introduced to combat the rapid topology change and high channel uncertainty in the dynamic network. Since the utility function is nonconvex and the probability constraints are intractable, the framework involving SCA and Bernstein approximation was developed to facilitate a convex optimization problem. To further maximize the systematic SE and EE in the imperfect CSI, two RPC algorithms based on the fixed price C and the optimal price C^* were proposed. Despite the unfavorable impact of Doppler effect on the average SE/EE and link reliability, the proposed clustering method and RPC were proved to be effective through the simulation results. Besides, a proper price C and a reasonable maximal cluster size were recommended to achieve the desired SE and EE performances. The design framework offers meaningful reference for future green and robust vehicular network.

Appendix A

When $i \neq j$, $\tilde{g}_{ij}$ are independent exponential random variables with mean $H_{ij}(1-\varpi_{ij}{}^2)$ and are assumed to be bounded on segments $[0, 2H_{ij}(1-\varpi_{ij}^2)]$. Then, $\alpha_{ij}=\beta_{ij}=H_{ij}(1-\varpi_{ij}^2)$. Through (11), $\xi_{ij}\in[-1,1]$ and the probability density function of ξ_{ij} is uniformly formulated as

$$f_{\xi_{ij}}(y)=\mathrm{e}^{-(y+1)}, y\in[-1,1] \tag{27}$$

Hence, the expectation and variance of ξ_{ij} are captured by

$$\begin{aligned}\mathbb{E}\{\xi_{ij}\}&=\int_{-1}^{1} y f_{\xi_{ij}}(y)dy=\int_{-1}^{1} y\mathrm{e}^{-(y+1)}dy\approx -0.271,\\ \mathbb{D}\{\xi_{ij}\}&=\int_{-1}^{1} y^2 f_{\xi_{ij}}(y)dy-\mathbb{E}^2\{\xi_{ij}\}\approx 0.25.\end{aligned} \tag{28}$$

See the Table I in [36], the values of μ_{ij}^+ and r_{ij} are set by

$$\begin{aligned}\mathbb{E}\{\xi_{ij}\}&\approx -0.271<\mu_{ij}^+=\frac{1}{2}<r_{ij}=\frac{\sqrt{2}}{2},\\ \mathbb{D}\{\xi_{ij}\}&\approx 0.25<r_{ij}^2=\frac{1}{2}<1.\end{aligned} \tag{29}$$

When (30) is adopted

$$W_{\mu,r}(t)\triangleq\begin{cases}\ln\left(\frac{(1-\mu)^2\mathrm{e}^{\frac{t(\mu-r^2)}{1-\mu}}+(r^2-\mu^2)\mathrm{e}^t}{1-2\mu+r^2}\right), \text{if } t\geq 0,\\ \ln\left(\frac{(1+\mu)^2\mathrm{e}^{\frac{t(\mu+r^2)}{1+\mu}}+(r^2-\mu^2)\mathrm{e}^{-t}}{1+2\mu+r^2}\right), \text{otherwise},\end{cases} \tag{30}$$

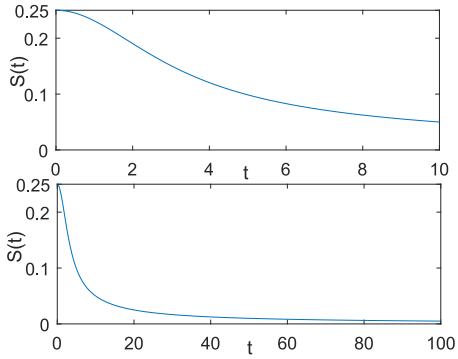

Fig. 11. Function images of $S(t)$.

the values of σ_{ij} can be given through solving

$$\sigma_{ij}=\min\left\{c\geq 0: W_{\mu_{ij}^+,r_{ij}}(t)\leq \mu_{ij}^+ t+\frac{c^2}{2}t^2,\ \forall t\right\}. \tag{31}$$

By combining (10) and (12), $f_n(\mathbf{p})\geq 0$ (i.e., $t\geq 0$). Hence, when $t\geq 0$, $\mu_{ij}^+=\frac{1}{2}$ and $r_{ij}=\frac{\sqrt{2}}{2}$, $W_{\mu_{ij}^+,r_{ij}}(t)=\ln(\frac{1}{2}+\frac{1}{2}\mathrm{e}^t)$ is used to obtain σ_{ij}.

Define

$$\begin{aligned}g(t)&=\frac{1}{2}t+\frac{c^2}{2}t^2,\ t\geq 0\\ f(t)&=g(t)-W_{\mu,r}(t)=\frac{1}{2}t+\frac{c^2}{2}t^2-\ln(\frac{1}{2}+\frac{1}{2}\mathrm{e}^t),\ t\geq 0.\end{aligned} \tag{32}$$

When $t=0$, $f(0)=0$, $f'(0)=0$. And $f'(t)$, the first-order derivative of $f(t)$, can be elaborated as

$$f'(t)=\frac{1}{2}+c^2 t-\frac{\mathrm{e}^t}{1+\mathrm{e}^t}. \tag{33}$$

To satisfy (31), $f'(t)\geq 0$ holds for any $t\geq 0$. Hence,

$$\begin{aligned}f'(t)\geq 0 \Longrightarrow c^2&\geq\frac{(\mathrm{e}^t-1)}{2(\mathrm{e}^t+1)t}\\ &=\frac{1}{t}\left(\frac{1}{2}-\frac{1}{1+\mathrm{e}^t}\right)>0, \forall t\geq 0.\end{aligned} \tag{34}$$

Let $S(t)=\frac{1}{t}(\frac{1}{2}-\frac{1}{1+\mathrm{e}^t})$, then $c^2\geq S(t)_{\max}$ holds for any $t\geq 0$. Through Fig. 11 and $\lim_{t\to\infty}\frac{(\mathrm{e}^t-1)}{2(\mathrm{e}^t+1)t}=0$, $S(t)_{\max}=\frac{1}{4}$ can be achieved at $t=0$. In fact, $\lim_{t\to 0}\frac{(\mathrm{e}^t-1)}{2(\mathrm{e}^t+1)t}=\frac{1}{4}$. Hence, $\sigma_{ij}=c_{\min}=\frac{1}{2}$ when $c\geq 0$ is required in (31).

Appendix B

To illustrate the feasible set of the convex problem (17) is a convex set, we define a function set $\mathbf{h}(\tilde{\mathbf{p}})=\mathbf{Q}^T\mathrm{e}^{\tilde{\mathbf{P}}}$, where $\mathbf{Q}=[q_{ij}]_{N\times N}$ $(q_{ij}=\chi_{ij}+\sqrt{2\ln(\frac{1}{\varepsilon})}\sigma_{ij}\alpha_{ij})$, the jth function of the function set, $h_j=\mathbf{q}_j^T\mathrm{e}^{\tilde{\mathbf{P}}}(\mathbf{q}_j=(q_{1j},\ldots,q_{j-1,j},0,q_{j+1,j},\ldots,q_{Nj})^T)$.

For $\forall j\in\mathcal{J}$, the Hessian Matrix $\mathbf{H}_{h_j}(\tilde{\mathbf{p}})$ of the second-order differentiable function h_j at any point $\mathrm{P}(\tilde{p}_1,\ldots,\tilde{p}_j,\ldots,\tilde{p}_N)$ in

the feasible domain can be expressed as a diagonal matrix,

$$\mathbf{H}_{h_j}(\tilde{\mathbf{p}}) = diag(q_{11}\mathrm{e}^{\tilde{p}_1}, \ldots, q_{j-1,j-1}\mathrm{e}^{\tilde{p}_{j-1}}, 0, q_{j+1,j+1}\mathrm{e}^{\tilde{p}_{j+1}}, \ldots, q_{NN}\mathrm{e}^{\tilde{p}_N}), \quad (35)$$

where $\mathbf{H}_{h_j}(\tilde{\mathbf{p}})$ is positive semi-definite $\forall j \in \mathcal{J}$. Hence, all function in the function set $\mathbf{h}(\tilde{\mathbf{p}})$ are strict convex functions.

Since the function h_j is convex and the corresponding transformed constraint set in (17) is one of the epigraphs about the function h_j, the corresponding transformed constraint set is a convex set. By the property of intersection of convex sets in [39], it can be proved that the intersection of the constraint set in (17) is also a convex set.

APPENDIX C

Sufficiency:The feasible set of the convex problem (17) is represented by $\mathcal{F}$. $\tilde{\mathbf{p}}^*$ is the optimal log-domain power vector with respect to the optimal price C^*, it indicates that

$$\tilde{C} \triangleq \frac{R_{s,lb}(\mathrm{e}^{\tilde{\mathbf{p}}^*})}{\sum_{i=1}^{N}\zeta_i \mathrm{e}^{\tilde{p}_i^*} + P_C} \geq \frac{R_{s,lb}(\mathrm{e}^{\tilde{\mathbf{p}}})}{\sum_{i=1}^{N}\zeta_i \mathrm{e}^{\tilde{p}_i} + P_C}, \forall(\tilde{\mathbf{p}}) \in \mathcal{F} \cap \mathcal{B}, \quad (36)$$

where $(\tilde{\mathbf{p}}^*)$ is the center of some concentric ball sets $\mathcal{B}$ with the different radius. Based on these, $(\tilde{\mathbf{p}}^*)$ is the optimal solution for $\tilde{C}$ in (17) due to

$$\begin{aligned} &R_{s,lb}(\mathrm{e}^{\tilde{\mathbf{p}}}) - \tilde{C}\left(\sum_{i=1}^{N}\zeta_i \mathrm{e}^{\tilde{p}_i} + P_C\right) \leq 0 \\ &= R_{s,lb}(\mathrm{e}^{\tilde{\mathbf{p}}^*}) - \tilde{C}\left(\sum_{i=1}^{N}\zeta_i \mathrm{e}^{\tilde{p}_i^*} + P_C\right), \forall(\tilde{\mathbf{p}}) \in \mathcal{F} \cap \mathcal{B}. \end{aligned} \quad (37)$$

Through (36) and (37), $\tilde{C}$ is the optimal price which can achieve the maximal EE with the optimal power vector $\tilde{\mathbf{p}}^*$, i.e., the equation $R_{s,lb}(\mathrm{e}^{\tilde{\mathbf{p}}^*}) - \tilde{C}(\sum_{i=1}^{N}\zeta_i \mathrm{e}^{\tilde{p}_i^*} + P_C) = 0$ holds. **Necessity** : Combining the equilibrium equation and the optimality at $(\tilde{\mathbf{p}}^*)$, we can obtain

$$\begin{aligned} &R_{s,lb}(\mathrm{e}^{\tilde{\mathbf{p}}}) - C^*\left(\sum_{i=1}^{N}\zeta_i \mathrm{e}^{\tilde{p}_i} + P_C\right) \\ &\leq R_{s,lb}(\mathrm{e}^{\tilde{\mathbf{p}}^*}) - C^*\left(\sum_{i=1}^{N}\zeta_i \mathrm{e}^{\tilde{p}_i^*} + P_C\right) = 0, \forall(\tilde{\mathbf{p}}) \in \mathcal{F} \cap \mathcal{B}. \end{aligned} \quad (38)$$

The inequality in (38) can be reformulated as follows:

$$\frac{R_{s,lb}(\mathrm{e}^{\tilde{\mathbf{p}}})}{\sum_{i=1}^{N}\zeta_i \mathrm{e}^{\tilde{p}_i} + P_C} \leq C^* = \frac{R_{s,lb}(\mathrm{e}^{\tilde{\mathbf{p}}^*})}{\sum_{i=1}^{N}\zeta_i \mathrm{e}^{\tilde{p}_i^*} + P_C}, \forall(\tilde{\mathbf{p}}) \in \mathcal{F} \cap \mathcal{B}. \quad (39)$$

Hence, it turns out that C^* which satisfies the equilibrium equation is the optimal price.

APPENDIX D

To prove this theorem, we first define $D(C(k)) = R_s(\mathrm{e}^{\tilde{\mathbf{p}}(k)}) - C(k)(\sum_{i=1}^{N}\zeta_i \mathrm{e}^{\tilde{p}_i(k)} + P_C)$. Since the utility maximization problem in (17) is proved to be concave, the inequality $D(C(k)) \geq R_s(\mathrm{e}^{\tilde{\mathbf{p}}(k-1)}) - C(k)(\sum_{i=1}^{N}\zeta_i \mathrm{e}^{\tilde{p}_i(k-1)} + P_C) = 0$ holds. Through the iteration of $C(k+1)$ in (26), we can obtain

$$\begin{aligned} D(C(k)) &= R_s(\mathrm{e}^{\tilde{\mathbf{p}}(k)}) - C(k)\left(\sum_{i=1}^{N}\zeta_i \mathrm{e}^{\tilde{p}_i(k)} + P_C\right) \\ &= \left(\sum_{i=1}^{N}\zeta_i \mathrm{e}^{\tilde{p}_i(k)} + P_C\right)(C(k+1) - C(k)) \geq 0. \end{aligned} \quad (40)$$

Due to $(\sum_{i=1}^{N}\zeta_i \mathrm{e}^{\tilde{p}_i(k)} + P_C) \geq 0$, we finally get $C(k+1) \geq C(k)$. Hence, $C(k)$ is monotonically increasing with respect to the iterative number k until the price converges.

Assume that the network price converges at $C(l) = \hat{C}, (l \geq k)$. The converged price sequence $\{C(l) = \hat{C}\}_{l\to\infty}$ are proved to be the optimal price by contradiction.

If $\hat{C}$ is considered as a non-optimal value, the equilibrium equation isn't held according to Theorem 1, that is

$$R_s(\mathrm{e}^{\tilde{\mathbf{p}}^*(l)}) - C(l)\left(\sum_{i=1}^{N}\zeta_i \mathrm{e}^{\tilde{p}_i^*(l)} + P_C\right) \neq 0. \quad (41)$$

By combining (25) and (41), we can obtain that

$$C(l) \neq \frac{R_s(\mathrm{e}^{\tilde{\mathbf{p}}^*(l)})}{\sum_{i=1}^{N}\zeta_i \mathrm{e}^{\tilde{p}_i^*(l)} + P_C} = C(l+1), \quad (42)$$

which isn't in conformity with the fact of $C(l) = C(l+1)$.

Based on these, the optimal price $C^* = \lim_{l\to\infty} C(l)$ satisfies the equilibrium equation (25).

REFERENCES

[1] K. Zheng *et al.*, "Reliable and efficient autonomous driving: The need for heterogeneous vehicular networks," *IEEE Commun. Mag.*, vol. 53, no. 12, pp. 72–79, Dec. 2015.

[2] Z. Zhou *et al.*, "Energy-efficient edge computing service provisioning for vehicular networks: A consensus ADMM approach," *IEEE Trans. Veh. Technol.*, vol. 68, no. 5, pp. 5087–5099, May 2019.

[3] K. Abboud, H. A. Omar, and W. Zhuang, "Interworking of DSRC and cellular network technologies for V2X communications: A survey," *IEEE Trans. Veh. Technol.*, vol. 65, no. 12, pp. 9457–9470, Dec. 2016.

[4] Z. Liu *et al.*, "Efficient QoS support for robust resource allocation in blockchain-based femtocell networks," *IEEE Trans. Ind. Informat.*, vol. 16, no. 11, pp. 7070–7080, Nov. 2020.

[5] Z. Zhou, F. Xiong, C. Xu, Y. He, and S. Mumtaz, "Energy-efficient vehicular heterogeneous networks for green cities," *IEEE Trans. Ind. Informat.*, vol. 14, no. 4, pp. 1522–1531, Apr. 2018.

[6] J. Mei *et al.*, "A latency and reliability guaranteed resource allocation scheme for LTE V2V communication systems," *IEEE Trans. Wireless Commun.*, vol. 17, no. 6, pp. 3850–3860, Mar. 2018.

[7] Z. Liu, Y. Xie, K. Y. Chan, K. Ma, and X. Guan, "Chance-constrained optimization in D2D-based yehicular communication network," *IEEE Trans. Veh. Technol.*, vol. 68, no. 5, pp. 5045–5058, May 2019.

[8] A. Filippi *et al.*, "IEEE 802.11p Ahead of LTE-V2V for safety applications," *Autotalks & NXP's Whitepaper*, Sep. 2017.

[9] A. Filippi *et al.*, "Why 802.11p Beats LTE and 5G for V2X," [Online]. Available: http://www.eenewsautomotive.com/design-center/why80211p-beats-lte-and-5g-v2x, Accessed: Jan. 18, 2018.

[10] H. Wang *et al.*, "VANET modeling and clustering design under practical traffic, channel and mobility conditions," *IEEE Trans. Commun.*, vol. 63, no. 3, pp. 870–881, Mar. 2015.
[11] Y. Xu, X. Zhao, and Y. Liang, "Robust power control and beamforming in cognitive radio networks: A survey," *IEEE Commun. Surv Tuts.*, vol. 17, no. 4, pp. 1834–1857, Dec. 2015.
[12] M. Hadded *et al.*, "TDMA-based MAC protocols for vehicular Ad Hoc networks: A survey, qualitative analysis, and open research issues," *IEEE Commun. Surv Tuts.*, vol. 17, no. 4, pp. 2461–2492, Jun. 2015.
[13] Y. Weidong, L. Wei, L. Pan, and S. Limin, "TDMA-based control channel access for IEEE 802.11p in VANETs," *Int. J. Distrib. Sensor Netw.*, vol. 10, no. 8, pp. 124–138, Aug. 2014.
[14] S. Cao and V. C. S. Lee, "A novel adaptive TDMA-based MAC protocol for VANETs," *IEEE Commun. Lett.*, vol. 22, no. 3, pp. 614–617, Mar. 2018.
[15] R. Zhang, X. Cheng, Q. Yao, C. X. Wang, Y. Yang, and B. Jiao, "Interference graph-based resource-sharing schemes for vehicular networks," *IEEE Trans. Veh. Technol.*, vol. 62, no. 8, pp. 4028–4039, Oct. 2013.
[16] P. Basu, N. Khan, and T. Little, "A mobility based metric for clustering in mobile ad hoc networks," in *Proc. Distrib. Comput. Syst. Workshop*, Mesa, AZ, Apr. 2001, pp. 413–418.
[17] S. Ucar *et al.*, "Multihop-cluster-based IEEE 802.11p and LTE hybrid architecture for VANET safety message dissemination," *IEEE Trans. Veh. Technol.*, vol. 65, no. 4, pp. 2621–2636, Apr. 2016.
[18] M. Ren *et al.*, "A unified framework of clustering approach in vehicular Ad Hoc networks," *IEEE Trans. Intell. Transp. Syst.*, vol. 19, no. 5, pp. 1401–1414, May 2018.
[19] Y. Ren, F. Liu, Z. Liu, C. Wang, and Y. Ji, "Power control in D2D-based vehicular communication networks," *IEEE Trans. Veh. Technol.*, vol. 64, no. 12, pp. 5547–5562, Dec. 2015.
[20] L. Liang, G. Y. Li, and W. Xu, "Resource allocation for D2D-enabled vehicular communications," *IEEE Trans. Commun.*, vol. 65, no. 7, pp. 3186–3197, Jul. 2017.
[21] K. Xiong, P. Fan, Y. Lu, and K. B. Letaief, "Energy efficiency with proportional rate fairness in multirelay OFDM networks," *IEEE J. Sel. Areas Commun.*, vol. 34, no. 5, pp. 1431–1447, May 2016.
[22] Z. Zhou, M. Dong, K. Ota, and C. Xu, "Energy-efficient matching for resource allocation in D2D enabled cellular networks," *IEEE Trans. Veh. Technol.*, vol. 66, no. 6, pp. 5256–5268, Jun. 2017.
[23] K. Yang, S. Martin, C. Xing, J. Wu, and R. Fan, "Energy-efficient power control for device-to-device communications," *IEEE J. Sel. Areas Commun.*, vol. 34, no. 12, pp. 3208–3220, Dec. 2016.
[24] M. Chiang, C. W. Tan, D. P. Palomar, D. ONeill, and D. Julian, "Power control by geometric programming," *IEEE Trans. Wireless Commun.*, vol. 6, no. 7, pp. 2640–2650, Jul. 2007.
[25] K. Singh and M. L. Ku, "Toward green power allocation in relay-assisted multiuser networks: A pricing-based approach," *IEEE Trans. Wireless Commun.*, vol. 14, no. 5, pp. 2470–2486, May 2015.
[26] Z. Zhou *et al.*, "Reliable task offloading for vehicular fog computing under information asymmetry and information uncertainty," *IEEE Trans. Veh. Technol.*, vol. 68, no. 9, pp. 8322–8335, Sep. 2019.
[27] A. Nemirovski and A. Shapiro, "Convex approximations of chance constrained programs," *SIAM J. Optim.*, vol. 17, no. 4, pp. 969–996, Apr. 2006.
[28] N. Y. Soltani, S.-J. Kim, and G. B. Giannakis, "Chance-constrained optimization of OFDMA cognitive radio uplinks," *IEEE Trans. Wireless Commun.*, vol. 12, no. 3, pp. 1098–1107, Mar. 2013.
[29] S. Wang, W. Shi, and C. Wang, "Energy-efficient resource management in OFDM-based cognitive radio networks under channel uncertainty," *IEEE Trans. Commun.*, vol. 63, no. 9, pp. 3092–3102, Sep. 2015.
[30] Y. Zhang and S. Wang, "Resource allocation for cognitive radio-enabled femtocell networks with imperfect spectrum sensing and channel uncertainty," *IEEE Trans. Veh. Technol.*, vol. 65, no. 9, pp. 7719–7728, Sep. 2016.
[31] S. Xiao, X. Zhou, Y. Y. Wu, G. Y. Li, and W. Guo, "Robust resource allocation in full-duplex-enabled OFDMA femtocell networks," *IEEE Trans. Wireless Commun.*, vol. 16, no. 10, pp. 6382–6394, Oct. 2017.
[32] L. Vasconcelos, A. B. Silva, Á. Seco, and J. Silva, "Estimating the parameters of Cowans M3 headway distribution for roundabout capacity analyses," *Baltic J. Road Bridge Eng.*, vol. 7, no. 4, pp. 261–268, Apr. 2012.
[33] M. Fiore and J. Härri, "The networking shape of vehicular mobility," in *Proc. 9th ACM MobiHoc*, 2008, pp. 261–272.
[34] T. Kim, D. J. Love, and B. Clerckx, "Does frequent low resolution feedback outperform infrequent high resolution feedback for multiple antenna beamforming systems?," *IEEE Trans. Signal Process.*, vol. 59, no. 4, pp. 1654–1669, Apr. 2011.
[35] L. Liang *et al.*, "Spectrum and power allocation for vehicular communications with delayed CSI feedback," *IEEE Wireless Commun. Lett.*, vol. 6, no. 4, pp. 458–461, Aug. 2017.
[36] A. Ben-Tal and A. Nemirovski, "Selected topics in robust convex optimization," *Math. Prog.*, vol. 112, pp. 125–158, 2008.
[37] R. A. Horn, "The hadamard product," in *Proc. Symp. Appl. Math*, 1990, vol. 40, pp. 87–169.
[38] J. Papandriopoulos and J. Evans, "SCALE: A low-complexity distributed protocol for spectrum balancing in multi-user DSL networks," *IEEE Trans. Inf. Theory*, vol. 55, no. 8, pp. 3711–3724, Dec. 2009.
[39] S. Boyed and L. Vandenberghe, *Convex Optimization*, Cambridge, U.K.: Cambridge Univ. Press, 2004.
[40] R. D. Yates, "A framework for uplink power control in cellular radio systems," *IEEE J. Sel. Areas Commun.*, vol. 13, no. 7, pp. 1341–1347, Sep. 1995.

Yuan-ai Xie received the B.S. degree in automation from the North China University of Science and Technology, Tangshan, China, in 2016. He is currently working toward the Ph.D. degree in control science and engineering with Yanshan University, Qinhuangdao, China. His current research interests include wireless resource optimization, vehicular network and D2D communication.

Zhixin Liu (Member, IEEE) received the B.S., M.S., and Ph.D. degrees in control theory and engineering from Yanshan University, Qinhuangdao, China, in 2000, 2003, and 2006, respectively. He is currently a Professor with the Department of Automation, School of Electrical Engineering, Yanshan University, China. He visited the University of Alberta, Edmonton, AB, Canada, in 2009 to 2010. He has the author or coauthor more than 100 papers in technical journals and conference proceedings. His current research interests include performance optimization and energy-efficient protocol design in wireless sensor networks, resource allocation in cognitive radio networks, and vehicular network.

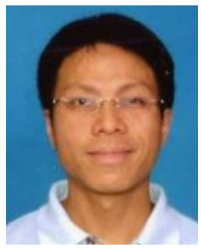

Kit Yan Chan (Member, IEEE) received the Ph.D. degree in computing from London South Bank University, U.K., in 2006. He is a Senior Lecturer with the Department of Electrical and Computer Engineering, Curtin University, Australia. He was a Full Time Researcher with The Hong Kong Polytechnic University (2004–2009) and Curtin University (2009–2013). He was the Guest Editor for IEEE TRANSACTIONS INDUSTRIAL INFORMATICS, APPLIED SOFT COMPUTING, NEUROCOMPUTING, ENGINEERING APPLICATIONS OF ARTIFICIAL INTELLIGENCE. His research interests include machine learning, pattern recognition and algorithm design.

Xinping Guan (Fellow, IEEE) received the B.S. degree in mathematics from Harbin Normal University, Harbin, China, in 1986 and the M.S. degree in applied mathematics and the Ph.D. degree in electrical engineering from the Harbin Institute of Technology, in 1991 and 1999, respectively. He is currently a Professor with the Department of Automation, School of Electronic, Information, and Electrical Engineering, Shanghai Jiao Tong University, Shanghai, China. He is the author or coauthor more than 200 papers in mathematical and technical journals. His current research interests include wireless sensor networks, networking control system, robust control, and intelligent control for nonlinear systems.